*Stanford Exploration Project, Report SERGEY, November 9, 2000, pages 313–??*

# The time and space formulation of azimuth moveout

*Sergey Fomel and Biondo L. Biondi*[1]

**ABSTRACT**

Azimuth moveout (AMO) transforms 3-D prestack seismic data from one common azimuth and offset to different azimuths and offsets. AMO in the time-space domain is represented by a three-dimensional integral operator. The operator components are the summation path, the weighting function, and the aperture. To determine the summation path and the weighting function, we derive the AMO operator by cascading dip moveout (DMO) and inverse DMO for different azimuths in the time-space domain. To evaluate the aperture, we apply a geometric approach, defining AMO as the result of cascading prestack migration (inversion) and modeling. The aperture limitations provide a consistent description of AMO for small azimuth rotations (including zero) and justify the economic efficiency of the method.

## INTRODUCTION

Azimuth moveout (AMO) is by definition an operator that transforms common-azimuth common-offset seismic reflection data to different azimuths and offsets[2]. A constructive approach to AMO was proposed by Biondi and Chemingui (1994). According to this approach, an AMO operator is built by cascading the dip moveout (DMO) operator that transforms the input common-azimuth data to zero offset, and the inverse DMO that transforms the zero-offset data to a new offset and azimuth. Evaluating the cascade of the frequency-domain DMO and inverse DMO operators by means of the stationary phase technique produces the integral (Kirchhoff-type) 3-D AMO operator in the time-space domain.

The first part of this paper applies an analogous idea to construct the AMO operator from the time-space domain DMO and achieves the same result in a simpler way. Cascading DMO and inverse DMO allows us to evaluate the AMO operator's summation path and the corresponding weighting function. However, it is not sufficient for evaluating the third major component of the integral operator, that is, its aperture (range of integration). To solve this problem, we apply an alternative approach, that defines AMO as a cascade of 3-D migration (inversion) for particular common-azimuth and common-offset data and 3-D modeling for a different azimuth and offset. This definition resembles the viewpoint on DMO developed by

[1]**email:** sergey@sep.stanford.edu, biondo@sep.stanford.edu

[2]Here azimuth corresponds to the direction of a source-receiver pair, and offset is the distance between the source and the receiver.

Deregowski and Rocca (1981). As with the DMO case, the migration and modeling approach reveals the physics of the AMO aperture and limits its boundaries. It is the aperture limitation that allows us to overcome the paradoxical inconsistency between 2-D and 3-D AMO operators discussed by Biondi and Chemingui (1994). If the aperture is chosen properly, the AMO operator converges to the 2-D offset continuation limit as the azimuth rotation approaches zero. This remarkable fact supports the proof of economical efficiency of AMO in comparison with the prestack migration operator, which is known to have an unlimited aperture.

## CASCADING DMO AND INVERSE DMO IN TIME-SPACE DOMAIN

In this section, we present a new version of the AMO derivation. Since the entire derivation is performed in the time-space domain, it is more straightforward than the stationary phase technique developed for the same purpose by Biondi and Chemingui (1994).

Let $P_1(\mathbf{x_1}, t_1; \mathbf{h_1})$ be the input of an AMO operator (common-azimuth and common-offset seismic reflection data after normal moveout correction) and $P_2(\mathbf{x_2}, t_2; \mathbf{h_2})$ be the output. Here $\mathbf{x_i}$ $(i = 1, 2)$ are midpoint locations on the surface: $\mathbf{x_i} = \{x_i, y_i\}$, and $\mathbf{h_i}$ are half-offset vectors. The 3-D AMO operator has the following general form:

$$P_2(\mathbf{x_2}, t_2; \mathbf{h_2}) = \mathbf{D}_{t_2} \int\int w_{12}(\mathbf{x_1}; \mathbf{x_2}, \mathbf{h_2}, t_2)\; P_1(\mathbf{x_1}, t_2\,\theta_{12}(\mathbf{x_1}; \mathbf{x_2}, \mathbf{h_2}); \mathbf{h_1})\, d\mathbf{x_1}\,, \tag{1}$$

where $\mathbf{D}$ is the differentiation operator $\left(\mathbf{D}_t \equiv \frac{d}{dt}\right)$, $t_2\theta_{12}$ is the summation path, and $w_{12}$ is the weighting function. In this section we will evaluate $\theta_{12}$ and $w_{12}$ using the cascade of integral 3-D DMO and inverse DMO operators in the time-space domain. The idea of this derivation originated in Biondi and Chemingui's paper (1994), where it was applied with the frequency-domain DMO and inverse DMO operators. In the next section, we apply a new geometric approach to evaluate the AMO aperture (range of integration in (1)).

To derive (1) in the time-space domain, an integral (Kirchoff-type) DMO operator of the form

$$P_0(\mathbf{x_0}, t_0; \mathbf{0}) = \mathbf{D}^{1/2}_{-t_0} \int w_{10}(\mathbf{x_1}; \mathbf{x_0}, \mathbf{h_1}, t_0)\; P_1(\mathbf{x_1}, t_0\,\theta_{10}(\mathbf{x_1}; \mathbf{x_0}, \mathbf{h_1}); \mathbf{h_1})\, d\hat{x}_1 \tag{2}$$

is cascaded with an inverse DMO of the form

$$P_2(\mathbf{x_2}, t_2; \mathbf{h_2}) = \mathbf{D}^{1/2}_{t_2} \int w_{02}(\mathbf{x_0}; \mathbf{x_2}, \mathbf{h_2}, t_2)\; P_0(\mathbf{x_0}, t_2\,\theta_{02}(\mathbf{x_0}; \mathbf{x_2}, \mathbf{h_2}); \mathbf{0})\, d\hat{x}_0\,, \tag{3}$$

where $\mathbf{D}^{1/2}_t$ stands for the operator of half-order differentiation (equivalent to $(i\omega)^{1/2}$ multiplication in Fourier domain), $t_0\theta_{10}$ and $t_2\theta_{02}$ are the summation paths of the DMO and inverse DMO operators (Deregowski and Rocca, 1981):

$$\theta_{10}(\mathbf{x_1}; \mathbf{x_0}, \mathbf{h_1}) = \left(1 - \frac{(\mathbf{x_1} - \mathbf{x_0})^2}{\mathbf{h_1^2}}\right)^{-1/2}, \tag{4}$$

$$\theta_{02}(\mathbf{x_0}; \mathbf{x_2}, \mathbf{h_2}) = \left(1 - \frac{(\mathbf{x_0} - \mathbf{x_2})^2}{\mathbf{h_2^2}}\right)^{1/2}, \tag{5}$$

$w_{10}$ and $w_{02}$ are the corresponding weighting functions (amplitudes of impulse responses), $\hat{x}_1$ is the component of $\mathbf{x_1}$ along the $\mathbf{h_1}$ azimuth, and $\hat{x}_0$ is the component of $\mathbf{x_0}$ along the $\mathbf{h_2}$ azimuth. Integral operators (2) and (3) correspond to the high-frequency asymptotic (the geometrical seismic) description of the wave field. As shown by Stovas and Fomel (1993), operator (3) has an asymptotically equivalent form

$$P_2(\mathbf{x_2}, t_2; \mathbf{h_2}) = \int \tilde{w}_{02}(\mathbf{x_0}; \mathbf{x_2}, \mathbf{h_2}, t_2)\, \mathbf{D}^{1/2}_{-t_0} P_0(\mathbf{x_0}, t_2\, \theta_{02}(\mathbf{x_0}; \mathbf{x_2}, \mathbf{h_2}); \mathbf{0})\, d\hat{x}_0 \,, \tag{6}$$

where $\tilde{w}_{02} = w_{02}\sqrt{\theta_{02}}$.

Both DMO and inverse DMO operate on 3-D seismic data as 2-D operators, since their apertures are defined on a line. This implies that for a given input midpoint $\mathbf{x_1}$, the corresponding location of $\mathbf{x_0}$ must belong to the line going through $\mathbf{x_1}$, with the azimuth defined by the input offset $\mathbf{h_1}$. Similarly, $\mathbf{x_0}$ must be on the line going through $\mathbf{x_2}$ with the azimuth of $\mathbf{h_2}$ (Figure 1). These theoretical facts lead us to the following conclusion:

> *For a given pair of input and output midpoints $\mathbf{x_1}$ and $\mathbf{x_2}$ of the AMO operator, the corresponding midpoint $\mathbf{x_0}$ on the intermediate zero-offset gather is determined by the intersection of two lines drawn through $\mathbf{x_1}$ and $\mathbf{x_2}$ in the offset directions.*

Applying the geometric connection among the three midpoints, we can find the cascade of the DMO and inverse DMO operators in one step. For this purpose, it is convenient to choose an orthogonal coordinate system $\{x, y\}$ on the surface in such a way that the direction of the $x$ axis corresponds to the input azimuth (Figure 1). In this case the connection between the three midpoints is given by

$$y_0 = y_1 \;;\; x_0 = x_2 - (y_2 - y_1)\cot\varphi \,, \tag{7}$$

$$d\hat{x}_1 = dx_1 \;;\; d\hat{x}_0 = dy_1 \csc\varphi \,. \tag{8}$$

Substituting (2) into (6) and taking into account (8) produces the 3-D integral AMO operator (1), where

$$\begin{aligned} \theta_{12}(\mathbf{x_1}; \mathbf{x_2}, \mathbf{h_2}) &= \theta_{02}(\mathbf{x_0}; \mathbf{x_2}, \mathbf{h_2})\, \theta_{10}(\mathbf{x_1}; \mathbf{x_0}, \mathbf{h_1}) = \left|\frac{\mathbf{h_1}}{\mathbf{h_2}}\right| \sqrt{\frac{\mathbf{h_2^2} - (\mathbf{x_2} - \mathbf{x_0})^2}{\mathbf{h_1^2} - (\mathbf{x_1} - \mathbf{x_0})^2}} = \\ &= \left|\frac{\mathbf{h_1}}{\mathbf{h_2}}\right| \sqrt{\frac{\mathbf{h_2^2}\sin\varphi^2 - (y_2 - y_1)^2}{\mathbf{h_1^2}\sin\varphi^2 - ((x_2 - x_1)\sin\varphi - (y_2 - y_1)\cos\varphi)^2}} \,, \end{aligned} \tag{9}$$

$$w_{12}(\mathbf{x_1}; \mathbf{x_2}, \mathbf{h_2}, t_2) =$$

$$= w_{02}(\mathbf{x_0}; \mathbf{x_2}, \mathbf{h_2}, t_2)\; w_{10}(\mathbf{x_1}; \mathbf{x_0}, \mathbf{h_1}, t_2\, \theta_{02}(\mathbf{x_0}; \mathbf{x_2}, \mathbf{h_2}))\, \frac{\csc\varphi}{\sqrt{\theta_{02}(\mathbf{x_0}; \mathbf{x_2}, \mathbf{h_2})}} \,, \tag{10}$$

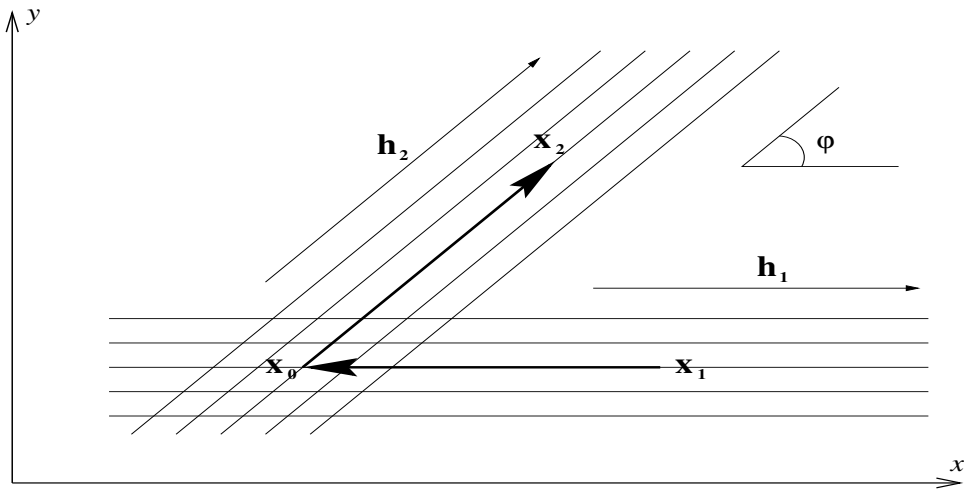


Figure 1: Geometric relationships between input and output midpoint locations in AMO. txamo-amox12 [NR]

$d\mathbf{x_1} = dx_1\,dy_1$. Equation $t_1 = t_2\,\theta_{12}(\mathbf{x_1};\mathbf{x_2},\mathbf{h_2})$ is the same as equation (4) in (Biondi and Chemingui, 1994) except for a different notation. The weighting function of the derived AMO operator ($w_{12}$) depends on the weighting functions of DMO and inverse DMO that are involved in the construction. In Appendix A, we apply equation (10) to two popular versions of the DMO weighting functions that correspond to Hale's (1984) and Zhang's (1988) DMO operators.

Deriving formula (9), we have to assume that the input and output offset azimuths are different ($\varphi \neq 0$). In the case of equal azimuths, AMO reduces to 2-D offset continuation (OC). The location of $\mathbf{x_0}$ in this case is not constrained by the input and output midpoints and can take different values on the line. Therefore the superposition of DMO and inverse DMO for offset continuation is a convolution on that line. To find the summation path of the OC operator, we should consider the envelope of the family of traveltime curves (where $x_0$ is the parameter of a curve in the family):

$$t_1 = t_2\,\theta_{12}(x_1;x_2,h_2) = t_2 \left|\frac{h_1}{h_2}\right| \sqrt{\frac{h_2^2-(x_2-x_0)^2}{h_1^2-(x_1-x_0)^2}}\,. \tag{11}$$

Solving the envelope condition

$$\frac{\partial \theta_{12}}{\partial x_0} = 0 \tag{12}$$

with respect to $x_0$ produces

$$x_0 = \frac{(\Delta x)^2 + h_2^2 - h_1^2 + \mathrm{sign}\left(h_1^2-h_2^2\right)\sqrt{\left((\Delta x)^2-h_1^2-h_2^2\right)^2 - 4h_1^2h_2^2}}{2\,(\Delta x)}\,, \tag{13}$$

where $\Delta x = x_1 - x_2$. Substituting (13) into (11), we get the explicit expression of the OC summation path:

$$t_1 = \begin{cases} \dfrac{t_2}{|h_2|}\sqrt{\dfrac{U+V}{2}} \text{ for } h_2 > h_1 \,, \\ t_2\,|h_1|\sqrt{\dfrac{2}{U+V}} \text{ for } h_2 < h_1 \,, \end{cases} \tag{14}$$

where $U = h_1^2 + h_2^2 - (\Delta x)^2$, and $V = \sqrt{U^2 - 4h_1^2 h_2^2}$. Equation (14) corresponds to formula (6) in (Biondi and Chemingui, 1994) (with a typo corrected). The same expression was obtained in a different way by Stovas and Fomel (1993). The apparent difference between the 2-D and 3-D solutions introduces the problem of finding a consistent description valid for both cases. Such a description is especially important for practical applications dealing with small angles of azimuth rotation, e.g. cable feather correction in marine seismics. The next section develops a way of solving this problem, which refers to the kinematic theory of AMO and follows the ideas that Deregowski and Rocca (1981) applied to DMO-type operators.

## AMO APERTURE: CASCADING MIGRATION AND MODELING

The impulse response of the AMO operators corresponds to a spike on the initial constant-offset constant-azimuth gather. Such a spike can physically occur in the case of a focusing ellipsoidal reflector whose focuses are coincident with the initial source and receiver locations (the impulse response of prestack common-offset migration). Therefore, the impulse response of AMO corresponds kinematically to a reflection from this ellipsoid. These considerations allow us to define AMO as the cascade of the 3-D common-offset common-azimuth migration and the 3-D modeling for a different azimuth and offset. An analogous point of view was developed for the 2-D case by Deregowski and Rocca (1981).

Let's consider the general symmetric ellipsoid equation

$$z(x,y) = \sqrt{R^2 - \beta\,(x-x_1)^2 - (y-y_1)^2}\,, \tag{15}$$

where $z$ stands for the depth coordinate, $R$ is the small semi-axis of the ellipsoid, and $\beta$ is a nondimensional parameter describing the stretching of the ellipse ($\beta < 1$). Deregowski and Rocca (1981) derived the following connections between the geometric properties of the reflector and the coordinates of the corresponding spike in the data:

$$R = \frac{v\,t_1}{2}\,;\ \beta = \frac{t_1^2}{t_1^2 + \frac{4\mathbf{h_1}^2}{v^2}}\,, \tag{16}$$

where $v$ is the wave velocity. The center of the ellipsoid is at the initial midpoint $\mathbf{x_1}$.

This section addresses the kinematic problem of reflection from the ellipsoid defined by (15). In particular, we are looking for the answer to the following question: *For a given elliptic*

*reflector defined by the input midpoint, offset, and time coordinates, what points on the surface can form a source-receiver pair valid for a reflection?* If a point in the output midpoint-offset space cannot be related to a reflection pattern, we should exclude it from the AMO impulse response defined in (1).

Fermat's principle provides a general method of solving the kinematic reflection problems. Consider a formal expression for the two-point reflection traveltime

$$t = \frac{\sqrt{(\boldsymbol{s}-\boldsymbol{\xi})^2 + z^2(\xi_x,\xi_y)}}{v} + \frac{\sqrt{(\boldsymbol{r}-\boldsymbol{\xi})^2 + z^2(\xi_x,\xi_y)}}{v}\,, \tag{17}$$

where $\boldsymbol{\xi} = \{\xi_x, \xi_y\}$ is the vertical projection of the reflection point to the surface, $\mathbf{s} = \{s_x, s_y\} = \mathbf{x_2} - \mathbf{h_2}$ is the source location, and $\mathbf{r} = \{r_x, r_y\} = \mathbf{x_2} + \mathbf{h_2}$ is the receiver location. According to Fermat's principle, the reflection ray path between two fixed points must correspond to the extremum value of the traveltime. Hence, in the vicinity of a reflected ray,

$$\frac{\partial t}{\partial \xi_x} = 0\,;\ \frac{\partial t}{\partial \xi_y} = 0\,. \tag{18}$$

Solving the system of equations (18) for $\xi_x$ and $\xi_y$ allows us to find the reflection ray path for a given source-receiver pair on the surface. The solution is derived in Appendix B to be

$$\xi_x = \frac{x_0 - \beta\, x_1}{1-\beta}\,, \tag{19}$$

$$\xi_y = y_1 + (x_0 - \xi_x)\cot\varphi - \frac{(y_2-y_1)\left[(x_0-\xi_x)^2 - \beta\,(x_1-\xi_x)^2 + R^2\right]}{\mathbf{h_2^2}\sin^2\varphi - (y_2-y_1)^2}\,, \tag{20}$$

where $x_0$ has the same meaning as in the preceding section and is defined by (7).

Since the reflection point is contained inside the ellipsoid, its projection obeys the evident inequality

$$\left(\xi_y - y_1\right)^2 \le R^2 - \beta\,(\xi_x - x_1)^2\ . \tag{21}$$

It is inequality (21) that defines the aperture of the AMO operator.

The AMO operator's contours for different azimuth rotation angles are shown in Figure 2. Comparing the results for the case of an unrealistically low velocity (the top two plots in Figure 2) and the case of a realistic velocity (the bottom two plots) clearly demonstrates the gain in the reduction of the aperture size achieved by the aperture limitation. The gain is especially spectacular for small azimuths. When the azimuth rotation approaches zero, the area of the 3-D aperture monotonously shrinks to a line, and the limit of the traveltime of the AMO impulse response (the inverse of (9)) approaches the offset continuation operator (14) (Figures 3). This means that taking into account the aperture limitations of AMO provides a consistent description valid for small azimuth rotations including zero (the offset continuation case). Obviously, the cost of an integral operator is proportional to its size. The size of the offset continuation operator cannot extend the difference between the offsets $||\mathbf{h_1}| - |\mathbf{h_2}||$. If

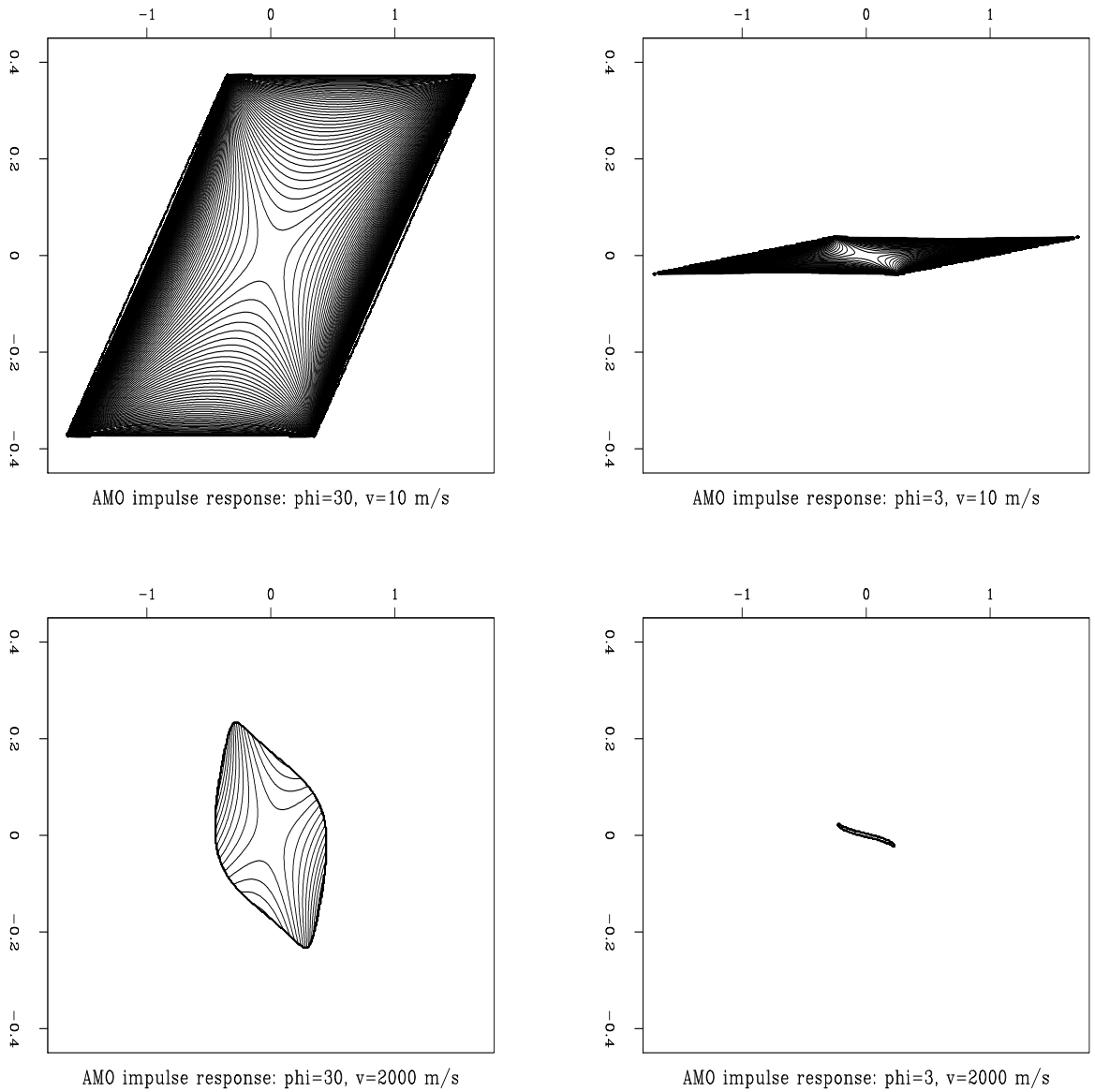


Figure 2: The AMO impulse response traveltime. Parameters: $|\mathbf{h1}| = 1000$ m, $|\mathbf{h2}| = 750$ m, $t_1 = 1$ sec. The top plots illustrate the case of an unrealistically low velocity ($v = 10$ m/s); on the bottom, $v = 2000$ m/s. On the left side the azimuth rotation $\varphi = 30°$; on the right, $\varphi = 3°$ txamo-amoapp [ER]

we applied DMO and inverse DMO explicitly, the total size of the two operators would be about $|\mathbf{h_1}|+|\mathbf{h_2}|$, which is substantially greater. This fact proves that in the case of small azimuth rotations the AMO price is less than those of not only 3-D prestack migration, but also 3-D DMO and inverse DMO combined (Canning and Gardner, 1992). Figure 4 shows the saddle shape of the AMO operator impulse response in a 3-D AVS display.

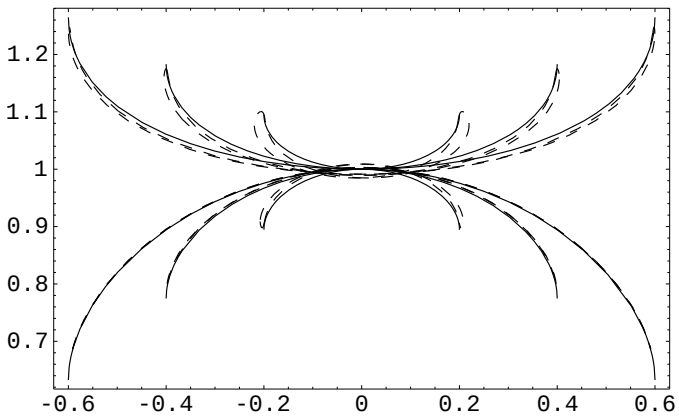


Figure 3: Traveltime curves of the impulse responses. The dashed lines indicate the AMO impulse response with an azimuth rotation of 3 degrees (projection on the $x$ plane); the solid lines, the 2-D offset continuation impulse response. txamo-amocom [CR]

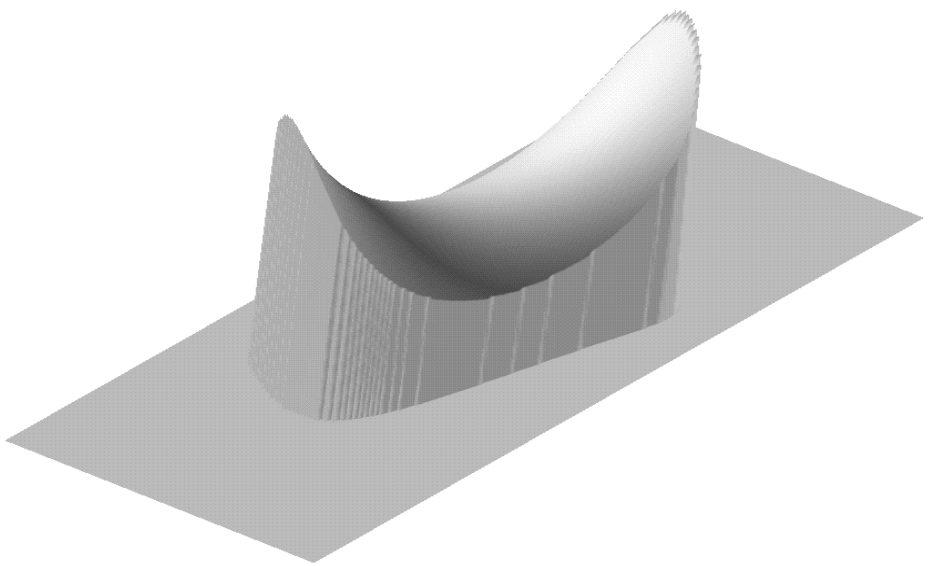

Figure 4: AMO impulse response traveltime in three dimensions (the AVS display). Parameters: $|\mathbf{h1}| = 1000$ m, $|\mathbf{h2}| = 750$ m, $t_1 = 1$ sec, $v = 2000$ m/s, $\varphi = 30°$. txamo-amoavs [NR]

## CONCLUSIONS

We have applied two different theoretical approaches to AMO to find a complete definition of the integral operator (1). Biondi and Chemingui (1994) proposed cascading the DMO and inverse DMO operators to define AMO in the frequency domain. The same approach is repeated here in a simpler way by transferring the analysis to the natural time-space domain. A new contribution to the evaluation of the AMO operator follows from applying a different approach, which extends the geometric theory of DMO (Deregowski and Rocca, 1981) to the AMO case. Cascading prestack migration and modeling allows us to evaluate the AMO operator aperture. The compactness of the AMO aperture indicates that the integral operator can be performed at a low cost and therefore promises economic benefits for its practical implementation.

## REFERENCES

Biondi, B., and Chemingui, N., 1994, Transformation of 3-D prestack data by Azimuth Moveout: SEP–**80**, 125–143.

Black, J. L., Schleicher, K. L., and Zhang, L., 1993, True-amplitude imaging and dip moveout: Geophysics, **58**, no. 1, 47–66.

Canning, A. J., and Gardner, G. H. F., 1992, Feathering correction for 3-D marine data: 62nd Annual Internat. Mtg., Soc. Expl. Geophys., Expanded Abstracts, 955–957.

Deregowski, S. M., and Rocca, F., 1981, Geometrical optics and wave theory of constant offset sections in layered media: Geophys. Prosp., **29**, no. 3, 374–406.

Hale, D., 1984, Dip-moveout by Fourier transform: Geophysics, **49**, no. 6, 741–757.

Ronen, J., 1987, Wave equation trace interpolation: Geophysics, **52**, no. 7, 973–984.

Stovas, A. M., and Fomel, S. B., 1993, Kinematically equivalent DMO operators: Presented at the Russian-Norwegian Oil Exploration Workshop III.

Zhang, L., 1988, A new Jacobian for dip moveout: SEP–**59**, 201–208.

## APPENDIX A

## AMO AMPLITUDE

The weighting function of the AMO operator can be determined from cascading the DMO and inverse DMO operators by means of equation (10). In the case of Hale's DMO (Hale, 1984)

and its adjoint (Ronen, 1987),

$$w_{10}(\mathbf{x_1};\mathbf{x_0},\mathbf{h_1},t_0) = \sqrt{\frac{t_0}{2\pi}}\,\frac{|\mathbf{h_1}|}{\mathbf{h_2^2}-(\mathbf{x_1}-\mathbf{x_0})^2}\,, \tag{A-1}$$

$$w_{02}(\mathbf{x_0};\mathbf{x_2},\mathbf{h_2},t_2) = \sqrt{\frac{t_2}{2\pi}}\,\frac{|\mathbf{h_2}|}{\mathbf{h_2^2}-(\mathbf{x_0}-\mathbf{x_2})^2}\,. \tag{A-2}$$

As follows from (A-1),(A-2), and (10),

$$w_{12}(\mathbf{x_1};\mathbf{x_2},\mathbf{h_2},t_2) = \frac{t_2}{2\pi}\times$$

$$\times\,\frac{|\mathbf{h_1}|\,|\mathbf{h_2}|\,\sin\varphi}{\left(\mathbf{h_1^2}\sin\varphi^2-((x_2-x_1)\sin\varphi-(y_2-y_1)\cos\varphi)^2\right)\left(\mathbf{h_2^2}\sin\varphi^2-(y_2-y_1)^2\right)}\,. \tag{A-3}$$

In the case of the so-called *true-amplitude* DMO (Black et al., 1993) and its asymptotic inverse,

$$w_{10}(\mathbf{x_1};\mathbf{x_0},\mathbf{h_1},t_0) = \sqrt{\frac{t_0}{2\pi}}\,\frac{\mathbf{h_1^2}+(\mathbf{x_1}-\mathbf{x_0})^2}{|\mathbf{h_1}|\left(\mathbf{h_1^2}-(\mathbf{x_1}-\mathbf{x_0})^2\right)}\,, \tag{A-4}$$

$$w_{02}(\mathbf{x_0};\mathbf{x_2},\mathbf{h_2},t_2) = \sqrt{\frac{t_2}{2\pi}}\,\frac{|\mathbf{h_2}|}{\mathbf{h_2^2}-(\mathbf{x_0}-\mathbf{x_2})^2}\,. \tag{A-5}$$

Inserting (A-4) and (A-5) into (10) yields

$$w_{12}(\mathbf{x_1};\mathbf{x_2},\mathbf{h_2},t_2) = \frac{t_2}{2\pi}\left|\frac{\mathbf{h_2}}{\mathbf{h_1}}\right|\times$$

$$\times\,\frac{\mathbf{h_1^2}\sin\varphi^2+((x_2-x_1)\sin\varphi-(y_2-y_1)\cos\varphi)^2}{\left(\mathbf{h_1^2}\sin\varphi^2-((x_2-x_1)\sin\varphi-(y_2-y_1)\cos\varphi)^2\right)\left(\mathbf{h_2^2}\sin\varphi^2-(y_2-y_1)^2\right)}\,. \tag{A-6}$$

## APPENDIX B

## DERIVING THE AMO APERTURE

This appendix describes the derivation of the main formulas for the aperture evaluation that follow from the Fermat principle (18). In order to avoid the algebraic complications of (18), we simplify the problem by taking into account the cylindrical symmetry of the ellipsoidal reflector (15).

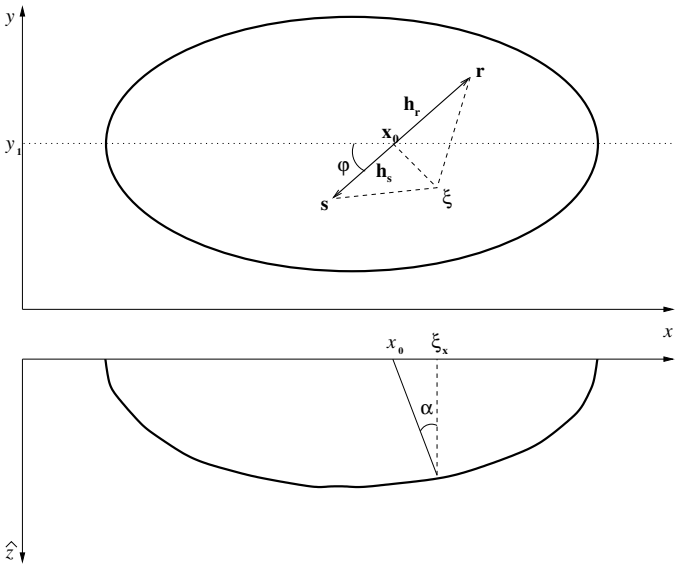


Figure B-1: Reflection from the ellipsoid of a prestack migration impulse response (a scheme). Top: Map view. Bottom: Section of the ellipsoid with the plane drawn through the central line and the reflection point. txamo-amosym [NR]

Consider a plane drawn through the reflection point and the central line of the ellipsoid (the axis of the cylindrical symmetry). This plane has to contain the central (normally reflected) ray from the reflector. This conclusion follows from the fact that all the normal reflections emerge at the central line because of the cylindrical symmetry, as shown in Figure B-1. The intersection of the 3-D reflector and the plane is the 2-D ellipse

$$\hat{z}(x) = \sqrt{R^2 - \beta\,(x - x_1)^2}\,. \tag{B-1}$$

The connection between the emergence point of the normal ray $x_0$ and the $x$ coordinate of the reflection point $\xi_x$ can be derived from the relationship evident in Figure B-1, as follows:

$$x_0 = \xi_x - \hat{z}\,(\xi_x)\tan\alpha = \xi_x + \hat{z}\,(\xi_x)\,\hat{z}'\,(\xi_x) = \xi_x\,(1-\beta) + \beta\,x_1\,. \tag{B-2}$$

Equation (B-2) allows us to evaluate $\xi_x$ in terms of $x_0$ and get (19). The emergence point of the normal ray $x_0$ corresponds to the midpoint on an imaginary zero-offset section ( with a coincident source and receiver). Therefore, the location of this point is determined for given input and output midpoints in accordance with expression (7).

Obviously, the reflection point has to be inside the ellipse (B-1). Therefore, its projection obeys the inequality

$$|\xi_x - x_1| \le \frac{R}{\sqrt{\beta}}\,. \tag{B-3}$$

As follows from (B-3), (B-2), and (16),

$$|x_0 - x_1| \le \frac{R\,(1-\beta)}{\sqrt{\beta}} = \frac{\mathbf{h_1^2}}{\sqrt{\frac{v^2 t_1^2}{2} + \mathbf{h_1^2}}}\,. \tag{B-4}$$

Inequality (B-4) is the known aperture limitation of the DMO operator (2) found by Deregowski and Rocca (1981). The equality in (B-4) is achieved when the reflection point is on the surface, where the reflector dip increases to 90 degrees.

Now the only unknown left in our problem is the $y$-coordinate of the reflection point $\xi_y$. To find this unknown, we substitute (19) into (17), choosing the convenient parameterization

$$\mathbf{s} = \mathbf{x_0} + \mathbf{h_s} \; ; \; \mathbf{r} = \mathbf{x_0} + \mathbf{h_r} \; , \tag{B-5}$$

where $\mathbf{h_r} - \mathbf{h_s} = 2\,\mathbf{h_2}$, and $\mathbf{h_r} + \mathbf{h_s} = 2\,(\mathbf{x_1} - \mathbf{x_0})$ (Figure B-1). The two-point traveltime function in (17) transforms to the form

$$\begin{aligned} t \;\; = \;\; & \frac{\sqrt{(x_0-\xi_x)^2 - \beta\,(x_1-\xi_x)^2 + R^2 + \mathbf{h_s^2} + 2\,\mathbf{h_s^2}\cdot(\boldsymbol{x_0}-\boldsymbol{\xi})}}{v} + \\ & + \frac{\sqrt{(x_0-\xi_x)^2 - \beta\,(x_1-\xi_x)^2 + R^2 + \mathbf{h_r^2} + 2\,\mathbf{h_r^2}\cdot(\boldsymbol{x_0}-\boldsymbol{\xi})}}{v} \; . \end{aligned} \tag{B-6}$$

Applying the second equation from (18), we get a simple linear equation for $\xi_y$, which has the explicit solution (20). From (19) and (20) one can find the reflection point location for given midpoint and offset. To find the limits of possible output midpoint locations, we constrain the reflection point to be inside the ellipsoid (15) similarly to the way we did in two dimensions when deriving (B-4). First, let's consider the case of $y_2 = y_1$ (the output midpoint $\mathbf{x_2}$ is on the line drawn through $\mathbf{x_1}$ in the direction of the input azimuth). In this case, combining expression (20) and inequality (21) produces

$$|x_0 - x_1| \le \frac{R\,(1-\beta)}{\sqrt{\beta + \beta^2\,\cot^2\varphi}} \; . \tag{B-7}$$

For any azimuth rotation angle $\varphi$ less than 90 degrees, the limitation (B-7) is smaller than that of the DMO operator (B-4). The difference increases with the decrease of the azimuth rotation, since the AMO aperture section on the line $y_2 = y_1$ monotonously shrinks to a point $x_2 = x_0 = x_1$ when $\varphi$ approaches zero. To extend this conclusion to the whole 3-D aperture, we can find the contour of the aperture by putting the reflection point at the edge of the ellipsoid (15), as follows:

$$\left(\xi_y - y_1\right)^2 = R^2 - \beta\,(\xi_x - x_1)^2 \tag{B-8}$$

and solving (20) for $y_2$. The aperture contour can then be defined by the system of parametric expressions

$$y_2\,(\xi_x) = y_1 + d\,(\xi_x)\,\sin\varphi \; , \tag{B-9}$$

$$x_2\,(\xi_x) = \xi_x\,(1-\beta) + \beta\,x_1 + d\,(\xi_x)\,\cos\varphi \; , \tag{B-10}$$

where

$$d\,(\xi_x) = \frac{d_y^2 + d_x^2 - \sqrt{\left(d_y^2 + d_x^2\right)^2 + 4\,\mathbf{h_2^2}\,\left(d_y\,\sin\varphi + d_x\,\cos\varphi\right)^2}}{2\,\left(d_y\,\sin\varphi + d_x\,\cos\varphi\right)} \; , \tag{B-11}$$

$d_x\,(\xi_x) = \xi_x - x_0 = \beta\,(\xi_x - x_1)$, and $d_y\,(\xi_x) = \xi_y - y_1$ is defined by (B-8).